Journal of Multidisciplinary Engineering Science and Technology (JMEST)
ISSN: 2458-9403
Vol. 8 Issue 10, October - 2021

KYAMOS Software – Cloud GPU InfiniBand tool for modeling COVID19

Antonis P. Papadakis, Aimilios Ioannou, Andreas Georgiou and Wasif Almady
KYAMOS LTD, 37 Polyneikis Street, Strovolos, 2047, Nicosia, Cyprus

***Abstract*— In this paper, we present an introduction to the corona virus and the way the virus behaves and transmits between humans. We then conduct a literature review of the research conducted in the transmission and propagation of the corona virus using computational fluid dynamics. We give special emphasis on the methods used, and most importantly, their speed and accuracy. Thereafter, we present the theory behind corona virus transmission and explain on how to model corona virus propagation. A mathematical model capable of capturing the corona particle propagation, and specifically the infected aerosols attached to the air propagated particles is presented together with its mathematical formulation. We explain thoroughly the Lattice Boltzmann Multiple Relaxation Time, together with the Smagorinsky Large Eddy Simulation model used to capture the sub-grid turbulent dynamics. Finally, the model implemented in CUDA is discussed and results of the corona virus propagation inside a room are presented. We investigate different realistic scenarios such as having two persons in a room breathing and talking and we produce different aerosol concentration plots and air particle speed velocities.**

Keywords—Lattice Boltzmann; Multiple Relaxation Time; incompressible flows;

I. INTRODUCTION

According to the World Health Organization, the coronavirus disease, also well known as COVID-19, is an infectious disease which is caused by the SARS-CoV-2 virus. In most cases, the virus causes mild to moderate respiratory illness and patients recover without requiring any special treatment. However, in some cases, especially when people that are infected have a medical illness record, they become seriously ill and require medical attention, with most of them requiring respiratory support. It affects mainly the elderly people and those which suffer with cardiovascular disease, diabetes, chronic respiratory disease, or cancer, and are more likely to develop serious illness. The majority of the people at an elder age are more likely to die from such a virus, however the virus is mutating, affecting younger age groups and causing serious illness, and sometimes death, as time progresses due to different mutations of the virus.

The virus is spread through an infected person's mouth and nose through actions such as sneezing, coughing, speaking, breathing or singing. The size of this infectious particles which transmit the virus varies from large respiratory droplets to smaller aerosols. Even though inhalation/exhalation of particles occurs within 1-2 m distance, the aerosols of an infected person move throughout an entire room or an indoor space at much larger distances, and it is suspected that they remain air-born, even hours after the infected person has emptied the premises. On the other hand, transmission of the virus can occur through contact of infectious surfaces, even though it is considered less likely. If one wishes to limit the chance of getting infected from the virus, one needs to limit the exposure time and distances of exposure to other people and inside rooms that could potentially encompass infectious particles through respiratory action of people that occupied the room before or of people that are currently in that room.
Since the main means of virus transmission is through the respiratory action, it is imperative to be able to comprehend the spreading of these infectious particles in closed rooms. Today, we have the necessary tools using numerical modeling to model the propagation of these particles and study their concentration and spreading inside closed rooms.

II. LITERATURE REVIEW OF CORONA VIRUS CFD SIMULATIONS

Due to the corona virus outbreak, there has been recently a number of papers related to the study of the corona virus. A great number of these papers focuses on the propagation of these infectious particles through simulation and specifically computational fluid dynamics simulations. In this section, we describe the work recently performed on the corona virus infection propagation and discuss the findings of the research and scientific community.
In a paper by Mariam et al. [1], it is suggested that the airborne transmission of the COVID-19 virus is the major mode of transmission and its spatial transmission in an indoor typical office room is conducted through CFD simulation. Different respiratory actions are investigated of the infectious particles and the density profiles at a distance of 2 m in front of the emitter at 3 different ventilation rates (4, 6, and 8 air changes per hour (ACH)) were estimated for different combinations of inlet–outlet positions and emitter–receptor configurations. The authors utilize the

finite volume method, and specifically they solve the fully three-dimensional Navier-Stokes equations coupled with the RANS-type standard k-epsilon turbulence model. The study indicates that the ″rule of thumb based safe distance approach″ in itself is not adequate to prevent high concentration of particles persisting for long times and suggests ″air curtains″ as an appropriate approach to prevent prolonged high concentrations of infectious particles inside the room. Additionally, they stress that higher ventilation rate for better removal strategy is not always adequate to keep the room at low concentration rates.

In a paper by Bhattacharyya et al. [2], they investigate the effectiveness of air released from air-conditioning machines mixed with aerosol sanitizer in an attempt to reach every point of the space of the isolation room so as to kill the COVID-19 virus and protect medical workers. The laminar-transitional flow is simulated using the transition SST *k-ε* model, that involves four transport equations. It is suggested that high turbulent fields could potentially be an effective way of distributing sanitizer effectively all across the room, in an attempt to kill the COVID-19 virus.

In a paper by Obeidat [3], they use CFD simulations to evaluate the ventilation system design for an emergency department at a university hospital and identify the areas which were most susceptible to viral transmission, taking into consideration also the effect of pressure suction. They discovered that at critical areas such as overnight patient beds, surgical rooms, and resuscitation rooms, there was much higher air velocity, dispersion, and mixing levels than the rest of the spaces, with the possibility of the virus spreading in the surrounding areas to be increased. The finite volume method together with the k-epsilon model was used with 1.6 Billion mesh elements and each case study, lasted for 12h using the ANSYS 2020 CFX package.

Blocken et al. [4] study the potential aerodynamic effects introduced by a moving person and investigate whether a nearby person at 1.5 m distance or beyond could cause droplet transfer to another person. Therefore, computational fluid dynamics simulations of droplet movement and evaporation and of airflow around a runner, are performed. The movement of droplets emitted by an exhaling walking or running person nearby another walking or running person is simulated with different person configurations and it is found that the largest exposure of a person occurs to a trailing person which is in line behind the leading person, hence suggesting to avoid running on the slipstream of the leading person. Another suggestion is to follow the 1.5 m distance rule in either staggered or side by side arrangement. Otherwise, it is always best to keep much larger distances between persons to allow for the aerosol droplets to diffuse or evaporate.

Shekar et al. [5] model, using computational fluid dynamics, an isolation room with an effective ventilation system where a patient carrying acute air born disease is nurtured. The propagation of the droplets released due to sneezing of the patient are modeled by changing the various vent positions such as the air inlet and outlets, by using flow across the room to direct it towards the outlet while maintaining a negative pressure. The negative strain helps in confining the air-borne transmission of the deadly virus from spreading across the room and not letting them permeate outside the isolated region. An isolation room model has been studied using computational fluid dynamics, by setting up a discrete phase model by using injection spray modelling to observe the permeation of the virus droplets. The behavior of these aerosol droplets was altered by altering inlet and outlet locations and authors were able to minimize the spread of these harmful droplets by using the flow from the air inlet to go against the diffusing droplets.

Dbhouk and Drikakis [6] deploy computational multiphase fluid dynamics and heat transfer to investigate the transport, dispersion, and evaporation of saliva particles arising from a human cough. A three-dimensional, fully coupled Eulerian–Lagrangian technique including relative humidity, turbulent dispersion forces, droplet phase-change, evaporation, and breakup in addition to the droplet–droplet and droplet–air interactions, is deployed. Additionally, the wind speed effect on social distancing is also investigated. It was found that the wind speed greatly affects the distance travelled of the droplets with a distance of 6 m with wind speeds varying from of 4 to 15 km/h, whereas with no wind, the distance travelled was no more than the social distance recommended of 2 m.

There are simulations already out there that simulate the cough activity from humans and how this could affect the surrounding people. Some examples are people couching with and without a mask, sneezing and breathing close to other humans, virus spread while exercising, negative pressure rooms, operating ventilators, etc. However, there is a lack for a dedicated tool available to the general public that can be easily adjusted to anybody's needs by drag and drop actions that can produce meaningful results easily and efficiently, even for non-engineers and scientists. Our ability to produce demanding COVID19 simulations within minutes, makes us believe that KYAMOS tools is the new alternative to the very expensive software, that lack simplicity and speed, and the free open source software that lack friendliness and speed. KYAMOS software is committed in providing such a tool at affordable prices that can analyze such phenomena within minutes and not hours or days, using our cloud-based GPU InfiniBand infrastructure for convenience.

III. Literature Review on Lattice Boltzmann Turbulence Models

The LB methods have received immense interest recently when compared to the traditional finite difference, finite element and finite volume methods. Specifically, they provide a new attractive alternative which is generally applicable to transient flows. Instead of being based on a continuum assumption of

the macroscopic fluid properties, it uses a mesoscopic kinetic description from the Boltzmann equation. In contrast to the traditional methods above, there is no need for the solution of matrices which are ill-conditioned and it is ideal for parallelization, especially on the GPUs.

A review from Perumal et al. [7] states that the LB method has excellent numerical stability and constitutive versatility, hence receiving tremendous impetus with its spectacular use in incompressible and compressible fluid flow and heat transfer problems. From a computational point of view, LB equations can be solved locally, explicitly, and efficiently on parallel computers.

Wang [8] deploys a 3D model using the LB-MRT method for Large Eddy Simulation of urban boundary layer atmospheric flows and the simulations compare favorably to both laboratory studies in terms of the mean wind fields. Most importantly, they demonstrate that the numerical implementation using a GPU, show that real-time simulations are achieved. The Tesla V100 card is demonstrated to be 392 times faster than a single CPU processor. They discuss the fact that the LB is inherently adaptable to parallel processing, allowing one to take advantage of massively parallel computer architectures such as graphics processing units (GPUs). Moreover, they discuss that implementation of complex boundary conditions is straightforward and is easier than in classical methods [9] and LB has the potential to achieve real-time simulations on a typical desktop or laptop with a modern GPU for large computational domains with several millions of computation grid points [10], [11], [12], and [13]. Furthermore, the generation of computational grids for complex surface boundaries is very easy, and simple interpolation on immersed boundary methods can be applied [14].

Yasduda et al. [15] compare the Entropic LB model and Quasi-equilibrium LB models against LBGK traditional model in a two-dimensional, incompressible, homogenous, isotropic turbulence model and compare the stability, accuracy and computational effort. They observe enhancement of stability by using ELBM and QELBM. Specifically, it was found that in the case of simulation using coarse grid, ELBM is more stable, and in the case of simulation at high Mach regions, QELBM is more stable.

Suga et al. [16] develop an accurate and robust LB method for calculating turbulent flows by direct and large eddy simulation. They utilize the D3Q27 model with an MRT scheme. To avoid unphysical kinks in turbulent quantities at grid interfaces by local mesh refinement, a correction method is developed.

Jin et al. [17] couple the LB with the MRT collision model in three-dimensions using the D3Q19 model to resolve intermittent behaviors on small scales in isotropic turbulent flows. The high-order scaling exponents of the velocity structure functions, the probability distribution functions of Lagrangian accelerations, and the local energy dissipation rates, are investigated. This validation provides a solid basis for using the LB method to study more complex processes that are sensitive to small scales in turbulent flows, such as the relative dispersion of pollutants and mesoscale structures of preferential concentration of heavy particles suspended in turbulent flows.

Chikatamarla et al. [18] present a three-dimensional direct numerical simulation (DNS) of the Kida vortex turbulent flow using a novel high-order LB model. It is shown that the LB-DNS method is a promising alternative for Direct Numerical Simulations (DNS), as it quantitatively captures all the computed statistics of fluid turbulence.

Chen [19] conducts a LB simulation of a two-dimensional turbulent flow around NACA0012 airfoil using the MRT method incorporated with Spalart-Allmaras (SA) turbulence model with adaptive meshing. According to the results, LB gives pretty good predictions, and quite flexible domain size can be accepted, if the far field boundary condition is well posed. Compared to the 3D LES-LB simulations, two-dimensional LB with SA turbulent model is of lower computational load, but with good accuracy.

Youssef et al. [20] study turbulent flows around obstacles at high Reynolds number using the LB method and specifically the D2Q9 model, for modeling fluid flow in a horizontal channel and validated with Poiseuille flow. Thereafter, the scheme is applied for the simulation of a flow around a square cylinder using Large Eddy Simulation (LES) at high Reynolds number using the Smagorinsky model and verified with experimental data.

Jahanshaloo et al. [21] perform a review of the various LB methods on three main groups of turbulence simulation: DNS, LES and RANS methods that could be potentially used for the simulation of turbulent flows in COVID19 applications, which show similar performance with the Navier-Stokes equations counterparts and are more convenient to implement due to their parallelable nature.

Koda et al. [22] study a three-dimensional LB method for turbulent flow simulations through large eddy simulations (LES). In achieving this goal, the 3D LB code was first applied to compute the laminar flow over two tandem cylinders. After validating against literature data, the program was used to study the aerodynamic effects of the early 3D flow structures by comparing between 2D and 3D simulations. It was found that the span-wise instabilities have a profound impact on the lift and drag forces, as well as on the vortex shedding frequency.

To conclude, we anticipate that the usage of state-of-the-art software and hardware for LB-COVID19 simulations that supports CUDA aware MPI with cloud-based, distributed GPU solutions will outstrip its conventional software counterparts, that utilize in the best-case scenario, desktop type GPU cards and pave the way for near, real-live simulations of large computationally intensive problems related to

COVID19 cough propagation, as well as other turbulent flow simulations in general.

IV. Mathematical Model of Corona Virus Simulations

A. Introduction

Lattice Boltzmann MRT can be used to solve three-types of equations, the incompressible Navier-Stokes, the advection-diffusion and the heat equations. Below, we analyze the solution of the above equations in the context of the LB-MRT method.

B. Incompressible air flow

Regarding the air particles, we need to solve the incompressible Navier-Stokes equations, which are the continuity and momentum equations as follows:

$$\boldsymbol{\nabla} \cdot \boldsymbol{u} = 0 \tag{1}$$

$$\frac{\partial \boldsymbol{u}}{\partial t} + (\boldsymbol{u}.\boldsymbol{\nabla})\boldsymbol{u} - \boldsymbol{\nabla} \cdot (\mu \boldsymbol{\nabla u}) + \frac{1}{\rho}\boldsymbol{\nabla} P = \boldsymbol{F} \tag{2}$$

where $\boldsymbol{u}$ is the velocity, μ is the viscosity, P is the pressure, ρ is the density and $\boldsymbol{F}$ is the force acting on the body. Through Chapman-Enskog analysis, the incompressible Navier-Stokes equations can be recovered from the Lattice Boltzmann equations with the following assumptions:

Since it is a common practice to use the pressure as an independent variable in the incompressible Navier-Stokes equation, we introduce a local pressure distribution function

$$P = \boldsymbol{c_s^2} \cdot \rho \tag{3}$$

with $\mathbf{c_s^2} = \frac{1}{3}$ in lattice units, where c_s is the speed of sound.

In order to conduct the LB simulations efficiently of the above equations, all the parameters are scaled according to a characteristic value and are made dimensionless.

C. Incompressible aerosol flow

The aerosols are solved using the advection-diffusion equation. The advection diffusion equation is:

$$\frac{\partial C}{\partial t} + \boldsymbol{\nabla} \cdot (C\boldsymbol{u}) - \boldsymbol{\nabla} \cdot (D\boldsymbol{\nabla} C) = S \tag{4}$$

which can also be written as:

$$\frac{\partial C}{\partial t} + \boldsymbol{\nabla} \cdot (C\boldsymbol{u}) - D\boldsymbol{\nabla^2} C = S \tag{5}$$

by assuming that the diffusion coefficient occurs homogeneously. The advection is a phenomenon as a result of the velocity of the fluid which transports the species along the streamlines of the flow, whereas the diffusion is a second order processes at which the concentration of the species spreads due to the differential in species concentration. These two phenomena can occur side by side, or only one of them can prevail, depending on the type of flow.

In the above equation, C is the concentration of species which in this case is the aerosols particles, t is the time, **u** is the velocity of the aerosols in vector form, D is the homogeneous diffusion coefficient and S is the source term of the equation.

One can utilize the incompressible Navier-Stokes equation solver for solving the advection-diffusion equation using the following assumptions [23]. Starting from the incompressible Navier-Stokes equations:

$$\frac{\partial(\rho \boldsymbol{u})}{\partial t} + \boldsymbol{\nabla}.(\boldsymbol{\rho u u} + \boldsymbol{PI}) - \mu\, \boldsymbol{\nabla^2}(\boldsymbol{\rho u}) = \boldsymbol{F} \tag{6}$$

One can make the following assumptions:

$$\rho \boldsymbol{u} \rightarrow C, \rho \boldsymbol{uu} + \boldsymbol{PI} \rightarrow C\boldsymbol{u}, \boldsymbol{\mu} \rightarrow \boldsymbol{D}, \boldsymbol{F} \rightarrow \boldsymbol{S} \tag{7}$$

which reverts to the advection-diffusion equation above, hence the same Lattice Boltzmann formulation for the incompressible Navier-Stokes can be used for the advection-diffusion equation, with the only difference that we do not have the incompressibility equation, hence the velocity must be input from another equation, which in this case, is calculated from the incompressible Navier-Stokes of air particles. In the case of the incompressible Navier-Stokes, there are two conserved variables, which are the density and the momentum, whereas in this case, it is only the density of the aerosol species. It is not necessary in the advection-diffusion case to be 2nd order accurate. Likewise with the incompressible Navier-Stokes equations, but only first order accurate, however in our models, we utilize identical schemes of second order accuracy for both models. An assumption that the aerosols are purely passive and they are just dragged along with the fluid is assumed, without affecting the fluid flow of the air particles in the room, which is usually the case of a diluted species where any collisions between the majority carries (air particles) and minority carries (aerosol particles) can be neglected.

D. Heat flow

One can also use similar notation to recover the heat equation, when the following substitutions are performed:

$$\rho \boldsymbol{u} \rightarrow T, \rho \boldsymbol{uu} + \boldsymbol{PI} \rightarrow T\boldsymbol{u}, \boldsymbol{\nu} \rightarrow \boldsymbol{k}, \boldsymbol{F} \rightarrow \boldsymbol{S} \tag{8}$$

to give:

$$\frac{\partial T}{\partial t} + \boldsymbol{\nabla} \cdot (T\boldsymbol{u}) - \boldsymbol{\nabla} \cdot (k\boldsymbol{\nabla} T) = S \tag{9}$$

or:

$$\frac{\partial T}{\partial t} + \boldsymbol{\nabla} \cdot (T\boldsymbol{u}) - k\boldsymbol{\nabla^2 T} = S \tag{10}$$

where T is the temperature, k is the thermal diffusivity and is a property that is related to the rate of heat transfer through a fluid due to molecular motion. In the Navier-Stokes equation modeling, there is the

Reynolds number, which is the defining dimensionless number, which is also used to dictate the behavior of fluid flows, but also to revert between different units in the simulations. Similarly to the Reynolds number, in advection-diffusion dominated problems, one can define the Peclet number as follows:

$$Pe = \frac{LU}{D} \tag{11}$$

where *L* is the characteristic length, *U* the characteristic velocity of the flow and *D* the diffusion coefficient. The Peclet number is a ratio of advection and diffusion and a large number dictates that the flow is advection dominated, whereas a small number dictates that it is diffusion dominated.

In the case of the heat equation, one can define the Prandtl number:

$$Pr = \frac{v}{k} \tag{12}$$

where *v* is the kinematic viscosity. It is basically the ratio of momentum transport and heat transport. The Prandtl number is an example of a dimensionless number that is an intrinsic property of a fluid. Fluids with small Prandtl numbers are free-flowing liquids with high thermal conductivity and are therefore a good choice for heat conducting liquids, such as liquid metals [24].

E. Equilibrium distribution function

It is worth noting that during the conversion of the incompressible Navier-Stokes to the Advection Diffusion Equation (ADE), only the 0th moment of the distribution function is conserved, whereas the 1st moment of the distribution function is not conserved i.e. the momentum is not conserved by collision since it is calculated externally such as from the Navier Stokes equation. Regarding the equilibrium distribution function, one can choose two equilibrium for the distribution functions, one with low order

$$f_i^{eq} = w_i C\left(1 + \frac{c_i . \boldsymbol{u}}{c_s^2}\right) \tag{13}$$

or one with higher order accuracy:

$$f_i^{eq} = w_i C\left(1 + \frac{\boldsymbol{c_i}.\boldsymbol{u}}{c_s^2} + \frac{(\boldsymbol{c_i}.\boldsymbol{u})^2}{2c_s^4} - \frac{\boldsymbol{u}.\boldsymbol{u}}{2c_s^2}\right) \tag{14}$$

and the conserved macroscopic concentration C is recovered by:

$$C = \sum_i f_i \tag{15}$$

In the corona simulations, we use the most accurate equilibrium function and no heat equation is included, hence we solve only the incompressible Navier-Stokes equations for air particles and advection diffusion equations for aerosols. The heat equation is included in this paper only for completeness and future reference, if one wishes to include heating effects in incompressible flows.

V. LARGE EDDY SIMULATION (LES)

A. Smagorinsky

The Smagorinsky model is the most widely used Large Eddy Simulation approach used in the Lattice Boltzmann-Multiple Relaxation simulations. It includes the turbulent viscosity as an extra term to the already existing laminar viscosity to calculate the total viscosity.

$$v_{tot} = v_o + v_t \tag{16}$$

The relationship between the non-dimensional relaxation time and the kinematic viscosity is:

$$v_o = \frac{1}{3}(\tau - 0.5)c^2\,\delta t \tag{17}$$

The turbulent viscosity is calculated to be:

$$v_t = (C_S \Delta)^2 \sqrt{2\sum S_{ij} S_{ij}} \tag{18}$$

which results to:

$$v_t = \frac{(C_S \Delta)^2}{\sqrt{2(S_{xx}S_{xx} + S_{yy}S_{yy} + S_{zz}S_{zz} + S_{xy}S_{xy} + S_{yz}S_{yz} + S_{zx}S_{zx})}} \tag{19}$$

where Δ is the discretization width or cut off length and is taken equal to 1 single spacing i.e. 1 in lattice units and C_s the Smagorinsky constant, which is taken equal to 0.1. The Smagorinsky constant can takes various values according to the problem being solved and it is set empirically usually varying between 0.1-0.2. It also uses the strain rate tensor S_{ij} which is a function of the spatial derivates of the filtered velocities as follows:

$$S_{ij} = \frac{1}{2}\left(\frac{\partial_{\bar{u}\,i}}{\partial x_j} + \frac{\partial_{\bar{u}\,j}}{\partial x_j}\right) \tag{20}$$

$$v_o + v_t = \frac{1}{3}\left(\tau + \tau_{eddy} - 0.5\right)c^2\,\delta t \tag{21}$$

From above, we can conclude that:

$$v_t = \frac{\tau_{eddy}}{3}c^2\,\delta t \tag{22}$$

B. Stress-rate tensor

For the D2Q9 model, the stress-rate tensors are calculated as follows:

$$S_{xx} = \frac{1}{4\rho\delta t}\left(s_1\, m_1^{(1)} + 3s_7 m_7^{(1)}\right) \tag{23}$$

$$S_{yy} = \frac{-1}{4\rho\delta t}\left(s_1 m_1^{(1)} - 3s_7 m_7^{(1)}\right) \tag{24}$$

$$S_{xy} = \frac{-3}{2\rho\delta t}\left(s_7 m_8^{(1)}\right) \tag{25}$$

For the D3Q15 model, the stress-rate tensors are calculated as follows:

$$S_{xx} = \frac{1}{2\rho\delta t}(s_1\, m_1^{(1)} + 3s_9 m_9^{(1)}) \quad (26)$$

$$S_{yy} = \frac{-1}{4\rho\delta t}(2s_1 m_1^{(1)} - s_9(m_9^{(1)} - 3m_{10}^{(1)}) \quad (27)$$

$$S_{zz} = \frac{-1}{4\rho\delta t}(2s_1 m_1^{(1)} - s_9(m_9^{(1)} + 3m_{10}^{(1)}) \quad (28)$$

$$S_{xy} = \frac{-3}{2\rho\delta t}(s_{11} m_{11}^{(1)}) \quad (29)$$

$$S_{yz} = \frac{-3}{2\rho\delta t}(s_{11} m_{12}^{(1)}) \quad (30)$$

$$S_{zx} = \frac{-3}{2\rho\delta t}(s_{11} m_{13}^{(1)}) \quad (31)$$

For the D3Q19 model, the stress-rate tensors are calculated as follows:

$$S_{xx} = \frac{-1}{38\rho\delta t}(s_1\, m_1^{(1)} + 19s_9 m_9^{(1)}) \quad (32)$$

$$S_{yy} = \frac{-1}{76\rho\delta t}(2s_1 m_1^{(1)} - 19s_9(m_9^{(1)} - 3m_{11}^{(1)})) \quad (33)$$

$$S_{zz} = \frac{-1}{76\rho\delta t}(2s_1 m_1^{(1)} - 19s_9(m_9^{(1)} + 3m_{11}^{(1)})) \quad (34)$$

$$S_{xy} = \frac{-3}{2\rho\delta t}(s_9 m_{13}^{(1)}) \quad (35)$$

$$S_{yz} = \frac{-3}{2\rho\delta t}(s_9 m_{14}^{(1)}) \quad (36)$$

$$S_{zx} = \frac{-3}{2\rho\delta t}(s_9 m_{15}^{(1)}) \quad (37)$$

In the above calculations for the strain rate tensors, we need to calculate derivatives of the momentums. In order to achieve this, we conduct forward, backward and center differentiation depending on the lattice points position. There are 27 distinct cases at which different derivatives should be accounted for in the cube box which need to be adjusted to conduct forward or backward differencing such as 12 sides, 8 corner points, 6 boundary faces. The majority of the points are of course internal mesh points where central differencing is applied.

C. Moments – Equilibrium and Non-Equilibrium

In the context of the Lattice Boltzmann method, there is a particularly efficient way to compute the matrix S_{ij} by calculating the non-equilibrium moments as follows:

$$f_{neq} = f - f_{eq} \quad (38)$$

Equation (38) can be used to compute the non-equilibrium moments used in the LES Smagorinsky model since f = Mf and f_{eq} is calculated through well-known equations according to the stencil being used. Below, we summarize the equilibrium moment equations used for various two and three-dimensional stencils.

D2Q9 equilibrium moments

The moment vectors for vector m is as follows:

$$\boldsymbol{m} = \left(\rho, e, \varepsilon, j_x, q_x, j_y, q_y, P_{xx}, P_{xy}\right)^T \quad (39)$$

where ρ is the fluid density, e is the energy, ε is related to the square of energy, j_x is the x-momentum, q_x is moment related to flux in the x-direction, j_y is the y-momentum, q_y is the moment related to flux in the y-direction, P_{xx} is the moment related to the stress-rate tensor term in the xx-direction and P_{xy} is the stress-rate tensor term related to the xy direction.

Moments ρ, j_x and j_y are the conserved moments, whereas e, ε, q_x, q_y, P_{xx}, P_{xy} are the non-conserved moments.

The equilibriums for the above nine moments are as follows:

$$m_0^{eq} = \rho \quad (40)$$

$$m_1^{eq} = -2\rho + 3(j_x^2 + j_y^2) \quad (41)$$

$$m_2^{eq} = \rho - 3(j_x^2 + j_y^2) \quad (42)$$

$$m_3^{eq} = j_x \quad (43)$$

$$m_4^{eq} = -j_x \quad (44)$$

$$m_5^{eq} = j_y \quad (45)$$

$$m_6^{eq} = -j_y \quad (46)$$

$$m_7^{eq} = j_x^2 - j_y^2 \quad (47)$$

$$m_8^{eq} = j_x j_y \quad (48)$$

and the momentums in the x and y-directions are defined as:

$$j_x = \rho u_x \quad (49)$$

$$j_y = \rho u_y \quad (50)$$

D3Q15 equilibrium moments

The moments in the D3Q15 case, are as follows:

$$\mathbf{m} = (\rho, e, \varepsilon, j_x, q_x, j_y, q_y, j_z, q_z, 3p_{xx}, p_{ww}, p_{xy}, p_{yz}, p_{xz}, m_{xyz}) \quad (51)$$

where ρ is the density, e is the energy, ε is the energy square, $\boldsymbol{j}(j_x, j_y, j_z)$ are the momentums in x, y, z directions, $\boldsymbol{q}(q_x, q_y, q_z)$ is the heat fluxes, p_{xx}, p_{ww}, p_{xy}, p_{yz}, p_{zx} are the stresses, and m_{xyz} is a 3rd order moment.

The equilibriums for the above 15 moments are as follows [25]:

$$m_0^{eq} = \rho \quad (52)$$

$$m_1^{eq} = -(\rho - rho) + \frac{1}{rho}(j_x^2 + j_y^2 + j_z^2) \quad (53)$$

$$m_2^{eq} = -\rho \quad (54)$$

$$m_3^{eq} = j_x \quad (55)$$

$$m_4^{eq} = -\frac{7}{3}j_x \quad (56)$$

$$m_5^{eq} = j_y \quad (57)$$

$$m_6^{eq} = -\frac{7}{3}j_y \quad (58)$$

$$m_7^{eq} = j_z \quad (59)$$

$$m_8^{eq} = -\frac{7}{3}j_z \quad (60)$$

$$m_9^{eq} = \frac{1}{rho}(2j_xj_x - (j_yj_y + j_zj_z)) \quad (61)$$

$$m_{10}^{eq} = \frac{1}{rho}(j_yj_y + j_zj_z) \quad (62)$$

$$m_{11}^{eq} = \frac{1}{rho}(j_xj_y) \quad (63)$$

$$m_{12}^{eq} = \frac{1}{rho}(j_yj_z) \quad (64)$$

$$m_{13}^{eq} = \frac{1}{rho}j_xj_z \quad (65)$$

$$m_{14}^{eq} = 0 \quad (66)$$

D3Q19 equilibrium moments

The moments in the D3Q19 case, are as follows:

$$\boldsymbol{m} = (\rho, e, \varepsilon, j_x, q_x, j_y, q_y, j_z, q_z, 3p_{xx}, 3\pi_{xx}, p_{ww}, \pi_{ww}, p_{xy}, p_{yz}, p_{xz}, m_x, m_y, m_z) \quad (67)$$

where ρ is the density, e is the energy, ε is the energy square, $\boldsymbol{j}(j_x, j_y, j_z)$ are the momentums in x, y, z directions, $\boldsymbol{q}(q_x, q_y, q_z)$ are the heat fluxes, p_{xx}, p_{ww}, p_{xy}, p_{yz}, p_{zx} are the stresses, and m_x, m_y, m_z are 3rd order moments and π_{xx} and π_{ww} are fourth-order moments derived from products between energy mode and normal stress mode.

The equilibriums for the above 19 moments are as follows:

$$m_0^{(1)} = \rho \quad (68)$$

$$m_1^{(1)} = \frac{38\delta t}{3s_1}\boldsymbol{\nabla}.\boldsymbol{j} \quad (69)$$

$$m_2^{(1)} = \frac{3(\omega_\varepsilon + 2)\delta t}{3s_2}\boldsymbol{\nabla}.\boldsymbol{j} \quad (70)$$

$$m_3^{(1)} = j_x \quad (71)$$

$$m_5^{(1)} = j_y \quad (72)$$

$$m_7^{(1)} = j_z \quad (73)$$

$$m_4^{(1)} = \frac{42\delta t}{63s_4}\partial_t\boldsymbol{j} + \frac{2(22 - 5\omega_e)\delta t}{63s_4}\boldsymbol{\nabla}\rho \quad (74)$$

$$m_6^{(1)} = \frac{42\delta t}{63s_4}\partial_t\boldsymbol{j} + \frac{2(22 - 5\omega_e)\delta t}{63s_4}\boldsymbol{\nabla}\rho \quad (75)$$

$$m_8^{(1)} = \frac{42\delta t}{63s_4}\partial_t\boldsymbol{j} + \frac{2(22 - 5\omega_e)\delta t}{63s_4}\boldsymbol{\nabla}\rho \quad (76)$$

$$m_9^{(1)} = \frac{-2\delta t}{3s_9}(3\partial_x j_x - \boldsymbol{\nabla}.\boldsymbol{j}) \quad (77)$$

$$m_{10}^{(1)} = \frac{-\delta t}{3s_{10}}(3\partial_x j_x - \boldsymbol{\nabla}.\boldsymbol{j}) \quad (78)$$

$$m_{11}^{(1)} = \frac{-2\delta t}{3s_9}(\partial_y j_y - 2\partial_z j_z) \quad (79)$$

$$m_{12}^{(1)} = \frac{-\delta t}{3s_{10}}(\partial_y j_y - 2\partial_z j_z) \quad (80)$$

$$m_{13}^{(1)} = \frac{-\delta t}{3s_9}(\partial_x j_y + \partial_y j_x) \quad (81)$$

$$m_{14}^{(1)} = \frac{-\delta t}{3s_9}(\partial_y j_z + \partial_z j_y) \quad (82)$$

$$m_{15}^{(1)} = \frac{-\delta t}{3s_9}(\partial_z j_x + \partial_x j_z) \quad (83)$$

$$m_{16}^{(1)} = 0 \quad (84)$$

$$m_{17}^{(1)} = 0 \quad (85)$$

$$m_{18}^{(1)} = 0 \quad (86)$$

VI. Results of Corona Virus Simuations

A. Introduction

The main reason for infectious transmission for corona virus is considered the small aerosols that attach into the air particles which remain air-born for long times in the room. For this purpose, we have decided to model their transmission and propagation inside a closed room of 4 x 4 x 4 m^3 size.

For testing purposes, we have placed a person at the edge of the room and assumed that is breathing from the mouth in and out at a characteristic frequency that humans inhale and exhale and study the propagation of the aerosols in the room. Since the aerosols are small particles and attach to the air particles which are inhaled or exhaled from the infectious person, we treat this simulation as a multiphysics solution which requires firstly the propagation of air particles inside the room, and secondly the aerosols which attach to these air-born particles. To model these two types of particles, one needs to solve a coupled system of equations and conduct a number of assumptions.

Since the airflow inside a room is considered to be an incompressible flow since the Mach number of the air flow velocity is well below a value of Mach 0.3, we utilize an incompressible solver where we assume that the air particles have incompressible behavior. To study incompressible flows, one of the most promising techniques is the Lattice Boltzmann method, which operates in the mesoscopic scale and has great accuracy and stability, and most importantly due its locality, it is highly parallelable. The incompressible equations for the Lattice Boltzmann will provide the air density and velocity of the particles. Since the air particles carry the aerosols inside a closed room, the velocity of the aerosols is identical to the velocity of the air particles and it is used as an input to the aerosol's propagation. For the solution of the aerosol's propagation, we deploy an advection-diffusion equation solution in the context of the Lattice Boltzmann, where the velocity of the aerosols is known.

Whenever there is a multiphysics simulation involved, likewise in this case, one must consider the different timescales of the species or particles involved. In the case of COVID-19, the time scales of the two particles are identical, and it is not necessary to conduct multiple steps of one species for a single step of the other species, therefore at each time step, both the aerosols and air particle propagation are modeled and advanced in time.

The model we deploy is considered a one-way simulation in the sense that there is no feedback from the aerosols back to the propagated air and only the other way around, hence it is a one-way effect in one direction i.e. from air particles to aerosols.

The benefits of Lattice Boltzmann in scaling the simulations, mostly through weak scaling, by introducing more GPU cards, when larger domains are used, provides a clear advantage to other traditional methods used in incompressible flows which are those of finite difference, finite element and finite volume methods.

Some assumptions are needed to be made regarding the respiratory action. First, one needs to assume the velocity of the outflow air from the mouth and also the breathing rate which is the frequency of breathing.

It is extremely difficult to study the aerosol propagation inside a room experimentally and also know both the densities as well as velocities in great detail as time passes by. Computational modeling has the ability to provide real live insight into the propagation of these aerosols particles and give qualitative, but most importantly quantitative values of the aerosol's physical characteristics. Different scenarios under different initial and boundary conditions can be implemented and studied in great fidelity both in space and time, which is impossible to be conducted experimentally. This is one of the reasons that the Computer Aided Engineering industry has an 8-10% growth rate, which is expected to increase even further, especially nowadays, where there is a great need for understanding of our environment in the mesoscopic and macroscopic scale to prevent global warming and prevent spreading of infectious diseases.

In this paper, our intention is not to study thoroughly different scenarios of COVID-19 simulations, but to present the theory and model used for the successful modeling of COVID-19 simulations and demonstrate KYAMOS software capability to capture these phenomena.

The authors intend to develop the software to be able to handle complex moving geometries and also treat a number of different boundary conditions and scenarios which are realistic so that real scenarios can thoroughly analyzed. This could potentially include multiple people breathing, running, coughing, sneezing and room boundary conditions such as open windows, air-conditions, air fans, connecting doors and multiple rooms, as well as ambient outside boundary conditions. These actions will be incorporated into a KYAMOS software module related to COVID-19 and will be easily and automatically set so that even non-engineers can build easily and quickly a realistic model of the COVID-19 propagation inside premises and assess the results, avoiding any science involvement from the customer. We will provide drag and drop capability of different size of persons, doors and windows, air-conditions with different inflow air capabilities, ground as well as ceiling fans, the ability to include chairs, desks and offices inside the premises. Finally, we intend to provide dynamic boundary conditions that will change their behavior through time such as people walking in the room etc.

B. Relaxation parameters

To produce the three-dimensional simulations, we have to choose the relaxation parameters for the MRT method. The parameters must obey the following rules: (a) sm_3, sm_5 and sm_7 must be the same, sm_4, sm_6 and sm_8 must be the same, sm_{10} and sm_{12} must be the same, and sm_{16}, sm_{17} and sm_{18} are very important parameters and affect stability. For, sm_{16}, sm_{17} and sm_{18}, we have experienced stable results from 1.5 to 1.8 values, however anything higher, caused instabilities in the simulations. The values that were used are as follows:

$$sm_0 = 1.0 \quad (87)$$

$$sm_1 = 1.19 \quad (88)$$

$$sm_2 = 1.4 \quad (89)$$

$$sm_3 = 1.0 \quad (90)$$

$$sm_4 = 1.2 \quad (91)$$

$$sm_5 = 1.0 \quad (92)$$

$$sm_6 = 1.2 \quad (93)$$

$$sm_7 = 1.0 \quad (94)$$

$$sm_8 = 1.2 \quad (95)$$

$$sm_{10} = 1.4 \quad (96)$$

$$sm_{12} = 1.4 \quad (97)$$

$$sm_{16} = 1.8 \quad (98)$$

$$sm_{17} = 1.8 \quad (99)$$

$$sm_{18} = 1.8 \quad (100)$$

whereas sm_9, sm_{11}, sm_{13}, sm_{14} and sm_{15} are calculated using the LES Smagorinsky method.

C. Aerosol density and velocity plots when speaking

In order to simulate the corona virus COVID19 propagation, we have simulated a 4x4x4 m^3 room with closed walls. In one case, two infected persons from COVID19 are talking, and in the other case, they are breathing in the room at the same time. One of the persons stands at the edge left of the room facing right and the other person stands in the middle of the room also facing right. We have also placed a small open window on the right-side wall to see the effect that an open window would have on the aerosol propagation. We have conducted simulations with and without the window present. The simulation parameters assumed are that the kinematic viscosity of air is 1.5×10^{-5} $m^2 s^{-1}$, that the maximum physical velocity is 0.9 ms-1 and 1.8 ms-1, respectively. The cross-sectional area of the mouth is assumed to be 4.907×10^{-4} m^2, and the volume of the mouth is 1×10^{-3} m^{-3}. During speaking, it is assumed that ¾ of the time, the person speaks and ¼ of the time, the person inhales, and that the period for the speech is 4.44 s. Regarding the breathing, we assume that we have a sinusoidal wave, with peak value of velocity of 1.4 ms^{-1}, whereas during speaking, the peak velocity is contact at 0.6 ms^{-1}, and -1.8 ms^{-1} while inhaling, according to Baeuer et al. [26].

Figs. 1-8 depict the simultaneous spreading of the aerosol particles in normalized values within the room, as time progresses in three-dimensions, when two people are speaking. We can see that aerosol particles slowly propagate within the room and the aerosols from the two persons speaking, quickly after 1,000 time steps, they mix with each other. Onwards, a bubble is created, where it expands outwards until heating the walls of the room and occupies the whole space of the room. Thereafter, the longer the time the two persons speak, the higher the density of the aerosol concentration is in the room. Figs. 9-14 depict the velocity in x-direction of the air particles in normalized values within the room, as time progresses in two-dimensional plots. One can observe that the air particle velocity experiences slight turbulent behavior. Also one can observe the positive and negative velocity profiles of the air particles when exhaling and inhaling, respectively. One can see the air particles swirling around the mouth as expected in great detail and one can perform thorough direct comparisons of distancing of people and objects and draw useful conclusions of the spreading of the air particles inside the room.

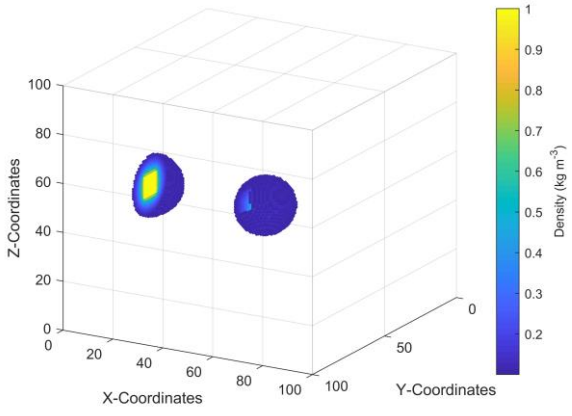

Fig. 1 Aerosol normalized density plot within a closed wall room when two people are speaking at the same time at 100 time steps.

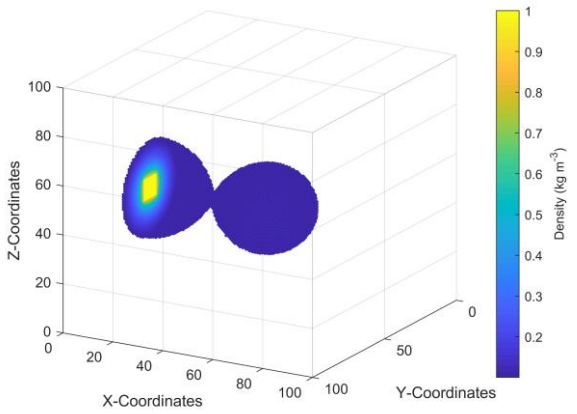

Fig. 2 Aerosol normalized density plot within a closed wall room when two people are speaking at the same time at 1,000 time steps.

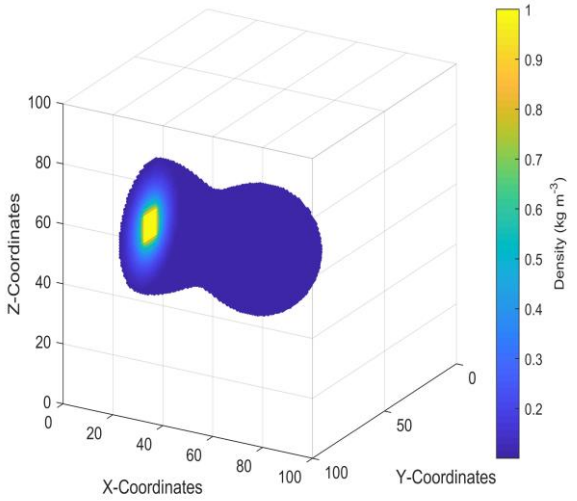

Fig. 3 Aerosol normalized density plot within a closed wall room when two people are speaking at the same time at 2,000 time steps.

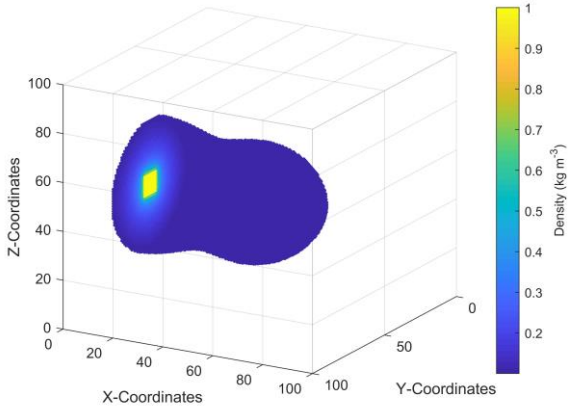

Fig. 4 Aerosol normalized density plot within a closed wall room when two people are speaking at the same time at 3,000 time steps.

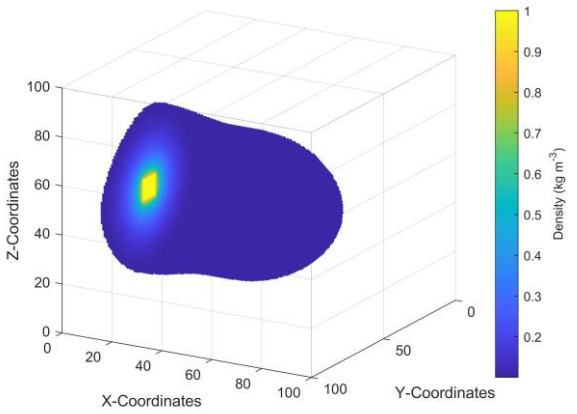

Fig. 5 Aerosol normalized density plot within a closed wall room when two people are speaking at the same time at 4,000 time steps.

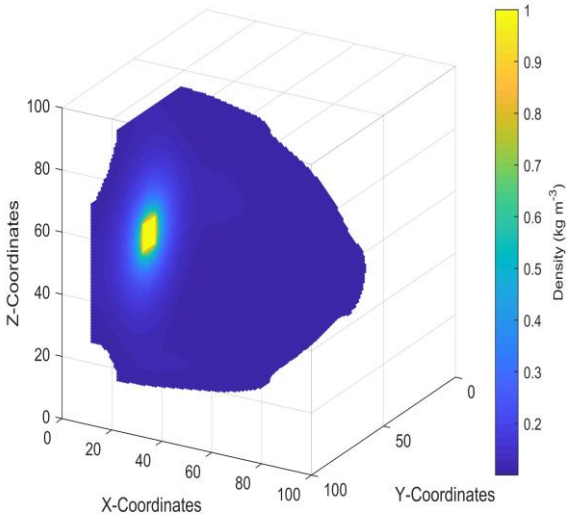

Fig. 6 Aerosol normalized density plot within a closed wall room when two people are speaking at the same time at 5,000 time steps.

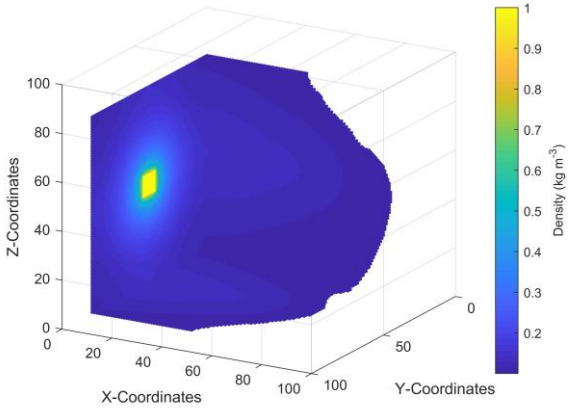

Fig. 7 Aerosol normalized density plot within a closed wall room when two people are speaking at the same time at 6,000 time steps.

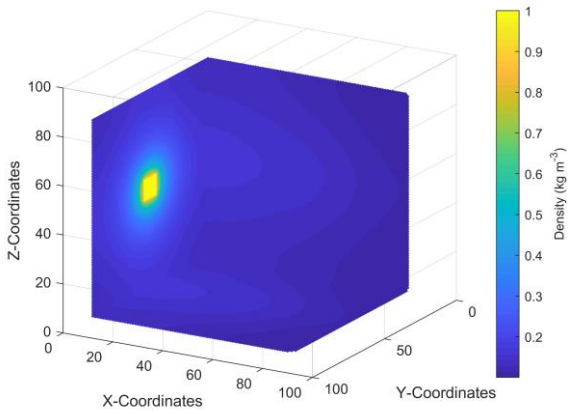

Fig. 8 Aerosol normalized density plot within a closed wall room when two people are speaking at the same time at 7,000 time steps.

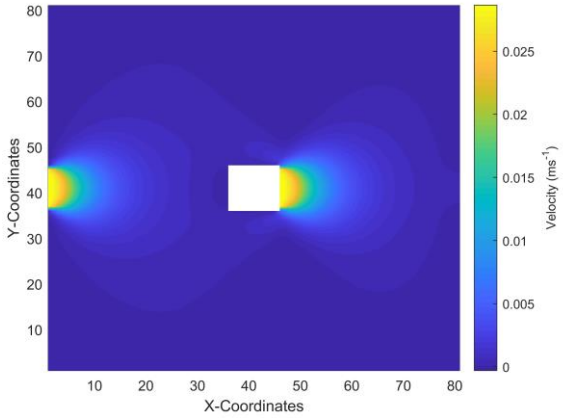

Fig. 9 Air velocity normalized plot within a closed wall room when two people are speaking at the same time at 100 time steps.

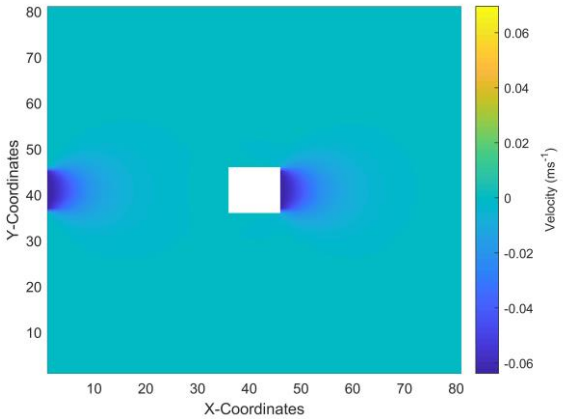

Fig. 10 Air velocity normalized plot within a closed wall room when two people are speaking at the same time at 1,000 time steps.

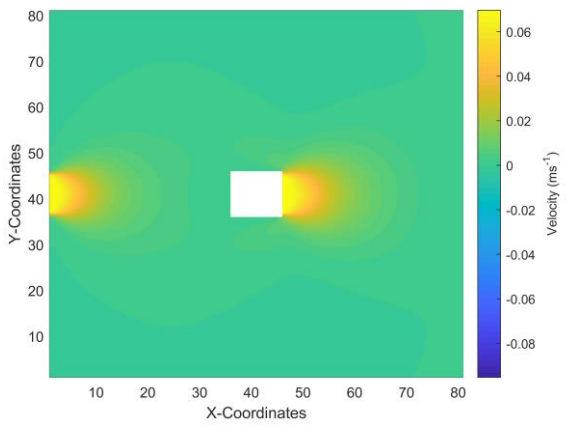

Fig. 11 Air velocity normalized plot within a closed wall room when two people are speaking at the same time at 2,000 time steps.

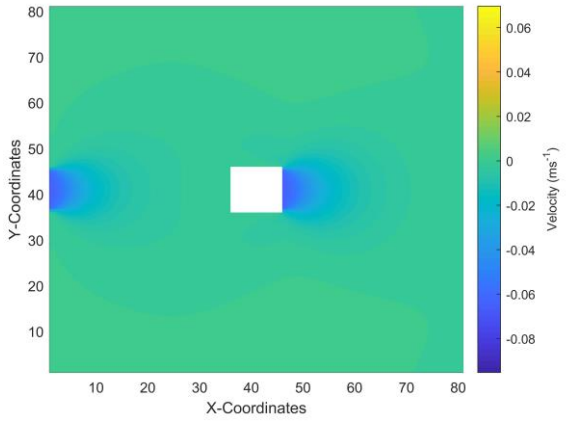

Fig. 12 Aerosol normalized density plot within a closed wall room when two people are speaking at the same time at 3,000 time steps.

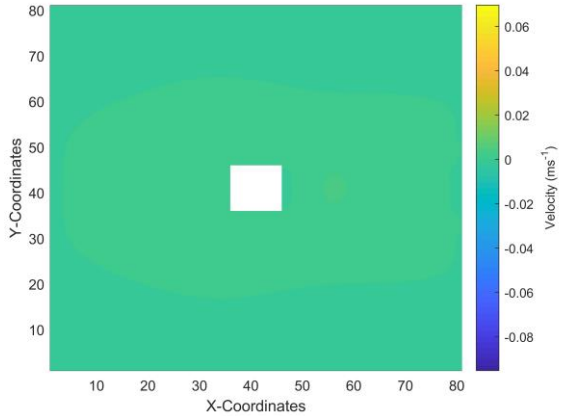

Fig. 13 Air velocity normalized plot within a closed wall room when two people are speaking at the same time at 4,000 time steps.

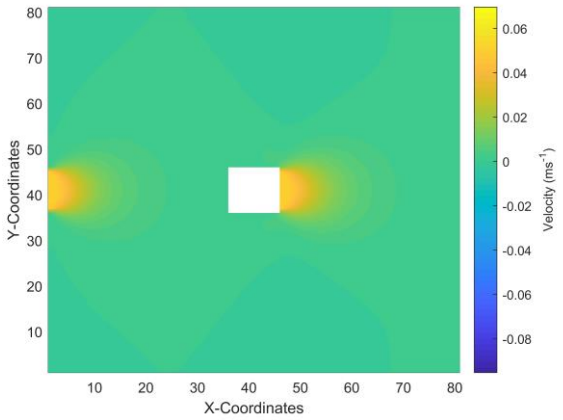

Fig. 14 Air velocity normalized plot within a closed wall room when two people are speaking at the same time at 5,000 time steps.

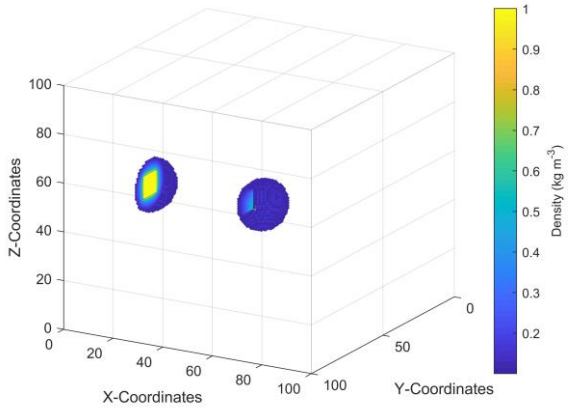

Fig. 15 Aerosol normalized density plot within a closed wall room when two people are breathing at the same time at 0 time steps.

D. Aerosol density and velocity plots when breathing

Fig. 15-19 depict the simultaneous spreading of the aerosol particles in normalized values within the room, when two infected people are breathing, as time progresses. The simulation is performed for a total time of 10,000 time steps. It is shown that in the beginning, the two persons infected aerosols' are separated and then they combine into one, and slowly expand outwards, until they occupy the whole room, similarly to the case when two people are speaking. The simulations show that there is no great difference whether people are breathing or speaking and actions must be taken inside a room, not only to keep open ventilation, but to provide a more drastic means of extracting air to the environment, such as by using air fans directed towards the outlet windows or by using air-conditioning. To conclude, the purpose of this paper was not to study the corona virus propagation and infection/mitigation measures in detail, hence we have limited our simulations to minimal analysis, but to demonstrate the capabilities of the algorithms, software and hardware. We will soon be releasing an extremely useful tool that utilizes state of the art algorithms (LB-MRT with LES), software (CUDA aware MPI) and hardware (cloud-based InfiniBand GPU) for the fight of COVID19 pandemic.

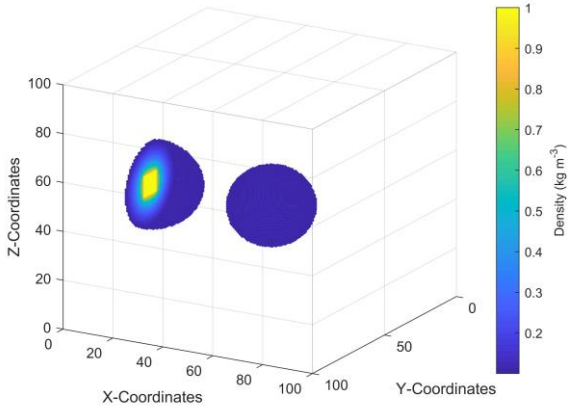

Fig. 16 Aerosol normalized density plot within a closed wall room when two people are breathing *at the same time at 500 time steps.*

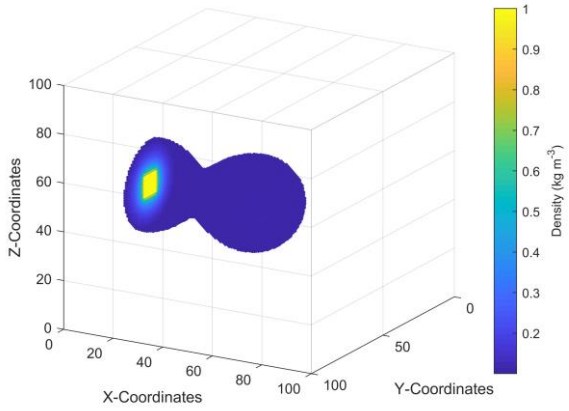

Fig. 17 Aerosol normalized density plot within a closed wall room when two people are breathing *at the same time at 1,500 time steps.*

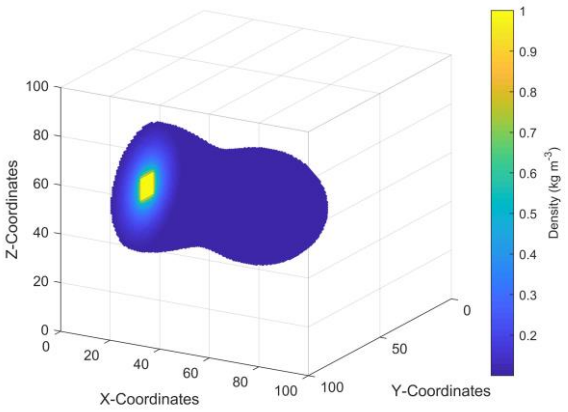

Fig. 18 Aerosol normalized density plot within a closed wall room when two people are breathing *at the same time at 2,500 time steps.*

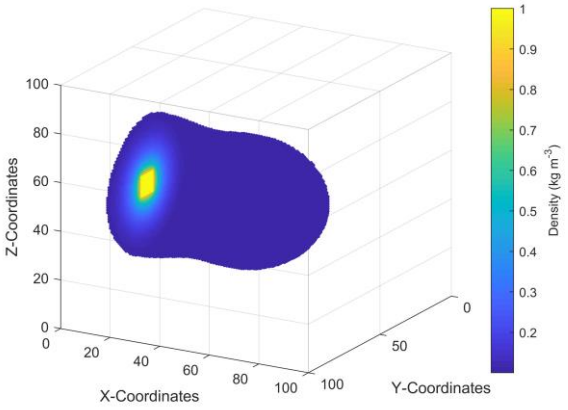

Fig. 19 Aerosol normalized density plot within a closed wall room when two people are breathing *at the same time at 3,500 time steps.*

VII. Conclusions

In this paper, we provided an introduction to corona virus issues and a literature review on CFD simulations was conducted. Thereafter, a literature review was presented on the turbulence models used for Lattice Boltzmann equations. Thereafter, the mathematical model used to analyze the air and aerosol propagation in a confined room was presented, as well as the model for the LES development using the Smagorinsky model. Thereafter, the results of the aerosol and air propagation inside a room were presented, in two different cases, when two people are talking and when two people are speaking in the room. It was shown that our Lattice Boltzmann MRT model is capable of capturing the corona virus propagation using GPUs very efficiently, since we were able to conduct 10,000 time steps, within only couple of minutes. We anticipate with the usage of faster GPU cards, the running times will decrease even further, paving the way for instant real live simulations with high fidelity in the future. Finally, we intend to release a specialized customize module within our software that will model efficiently the air and aerosol propagation in small, as well as large rooms or complexes, using our cloud based, InfiniBand GPU technology.

Acknowledgment

This work was co-funded by the European Regional Development Fund of the European Union and the Republic of Cyprus through the Research and Innovation Foundation (Project: CONCEPT-COVID/0420/0025).

References

[1] Mariam *et al.*, "CFD Simulation of the Airborne Transmission of COVID-19 Vectors Emitted during Respiratory Mechanisms: Revisiting the Concept of Safe Distance," *ACS Omega*, vol. 6, no. 26, pp. 16876-16889, 2021/07/06 2021.

[2] S. Bhattacharyya, K. Dey, A. R. Paul, and R. Biswas, "A novel CFD analysis to minimize the spread of COVID-19 virus in hospital isolation room," (in eng), *Chaos, solitons, and fractals*, vol. 139, pp. 110294-110294, 2020.

[3] B. Obeidat, O. F. Alrebei, I. A. Abdallah, E. F. Darwish, and A. Amhamed, "CFD Analyses: The Effect of Pressure Suction and Airflow Velocity on Coronavirus Dispersal," *Applied Sciences*, vol. 11, no. 16, p. 7450, 2021.

[4] B. Blocken, F. Malizia, T. Van Druenen, and T. Marchal, "Towards aerodynamically equivalent COVID19 1.5 m social distancing for walking and running," *preprint*, 2020.

[5] N. C. Shekar, B. Abhinay, C. R. Pavan, and R. Harish, "Controlling virus droplets diffusion in an isolated room using CFD," in *IOP Conference Series: Materials Science and Engineering*, 2021, vol. 1128, no. 1, p. 012003: IOP Publishing.

[6] T. Dbouk and D. Drikakis, "On coughing and airborne droplet transmission to humans," *Physics of Fluids*, vol. 32, no. 5, p. 053310, 2020.

[7] D. Arumuga Perumal and A. K. Dass, "A Review on the development of lattice Boltzmann computation of macro fluid flows and heat transfer," *Alexandria Engineering Journal*, vol. 54, no. 4, pp. 955-971, 2015/12/01/ 2015.

[8] Y. Wang, J. Decker, and E. R. Pardyjak, "Large-Eddy Simulations of Turbulent Flows around Buildings Using the Atmospheric Boundary Layer Environment–Lattice Boltzmann Model (ABLE-LBM)," (in English), *Journal of Applied Meteorology and Climatology*, vol. 59, no. 5, pp. 885-899, 01 May. 2020 2020.

[9] L.-S. Luo, M. Krafczyk, and W. Shyy, "Lattice Boltzmann method for computational fluid dynamics," *Encyclopedia of aerospace engineering*, vol. 56, pp. 651-660, 2010.

[10] C. Obrecht, F. Kuznik, L. Merlier, J.-J. Roux, and B. Tourancheau, "Towards aeraulic simulations at urban scale using the lattice Boltzmann method," *Environmental Fluid Mechanics*, vol. 15, no. 4, pp. 753-770, 2015/08/01 2015.

[11] M.-F. King *et al.*, "Modelling urban airflow and natural ventilation using a GPU-based lattice-Boltzmann method," *Building and Environment*, vol. 125, pp. 273-284, 2017/11/15/ 2017.

[12] S. Lenz *et al.*, "Towards real-time simulation of turbulent air flow over a resolved urban canopy using the cumulant lattice Boltzmann method on a

GPGPU," *Journal of Wind Engineering and Industrial Aerodynamics*, vol. 189, pp. 151-162, 2019/06/01/ 2019.

[13] N. Onodera, T. Aoki, T. Shimokawabe, and H. Kobayashi, "Large-scale LES wind simulation using lattice Boltzmann method for a 10 km× 10 km area in metropolitan Tokyo," *Tsubame ESJ*, vol. 9, pp. 2-8, 2013.

[14] Z. Guo and C. Shu, *Lattice Boltzmann method and its application in engineering*. World Scientific, 2013.

[15] T. Yasduda, T. Hashimoto, H. Minagawa, K. Morinishi, and N. Satofuka, "Efficient Simulation for Incompressible Turbulent Flow Using Lattice Boltzmann Model," *Procedia Engineering*, vol. 61, pp. 173-178, 2013/01/01/ 2013.

[16] K. Suga and Y. Kuwata, "Lattice Boltzmann Method for Turbulent Flows," Singapore, 2018, pp. 285-292: Springer Singapore.

[17] G. Jin, S. Wang, Y. Wang, and G. He, "Lattice Boltzmann simulations of high-order statistics in isotropic turbulent flows," *Applied Mathematics and Mechanics*, vol. 39, no. 1, pp. 21-30, 2018/01/01 2018.

[18] S. S. Chikatamarla, C. E. Frouzakis, I. V. Karlin, A. G. Tomboulides, and K. B. Boulouchos, "Lattice Boltzmann method for direct numerical simulation of turbulent flows," *Journal of Fluid Mechanics*, vol. 656, pp. 298-308, 2010.

[19] X.-P. Chen, "Applications of Lattice Boltzmann Method to Turbulent Flow Around Two-Dimensional Airfoil," *Engineering Applications of Computational Fluid Mechanics*, vol. 6, no. 4, pp. 572-580, 2012/01/01 2012.

[20] A. Youssef and M. El Hassan, "Turbulent Flow Modeling Using Lattice Boltzmann Method," EasyChair2516-2314, 2018.

[21] L. Jahanshaloo, E. Pouryazdanpanah, and N. A. Che Sidik, "A Review on the Application of the Lattice Boltzmann Method for Turbulent Flow Simulation," *Numerical Heat Transfer, Part A: Applications*, vol. 64, no. 11, pp. 938-953, 2013/12/01 2013.

[22] Y. Koda, "Lattice Boltzmann method for simulating turbulent flows," University of Waterloo, 2013.

[23] T. Krüger, H. Kusumaatmaja, A. Kuzmin, O. Shardt, G. Silva, and E. M. Viggen, "The lattice Boltzmann method," *Springer International Publishing*, vol. 10, no. 978-3, pp. 4-15, 2017.

[24] B. E. Rapp, *Microfluidics: modeling, mechanics and mathematics*. William Andrew, 2016.

[25] M. Krafczyk, J. Tölke, and L.-S. Luo, "Large-eddy simulations with a multiple-relaxation-time LBE model," *International Journal of Modern Physics B*, vol. 17, no. 01n02, pp. 33-39, 2003.

[26] M. Bauer, H. Köstler, and U. Rüde, "lbmpy: A flexible code generation toolkit for highly efficient lattice Boltzmann simulations," *arXiv preprint arXiv:2001.11806*, 2020.